2013-11

A Grid-Connected Multilevel Converter for Interfacing PV Arrays and Energy Storage Devices

Annual Conference of the IEEE Industrial Electronics Society, 39, 2013, Vienna, Austria
http://www.producao.usp.br/handle/BDPI/50026

A Grid-Connected Multilevel Converter for Interfacing PV Arrays and Energy Storage Devices

Giovani G. Pozzebon; Ricardo Q. Machado
Department of Electrical Engineering
São Carlos School of Engineering – USP
São Carlos, Brazil
pozzebon@ieee.org; rquadros@sc.usp.br

Simone Buso; Giorgio Spiazzi
Department of Information Engineering
University of Padova
Padova, Italy
simone.buso@dei.unipd.it; giorgio.spiazzi@dei.unipd.it

***Abstract*—This paper presents a design procedure and a control strategy for a grid-connected single-phase multilevel converter. The proposed system uses two series connected H-bridge modules, one fed by photovoltaic panels, the other by energy storage devices. The former switches at line frequency, while the latter operates in PWM. The system is designed to minimize the voltage stress on the switches, while the control strategy is such that a constant active power is delivered to the grid with high power factor, even if the energy produced by the photovoltaic panels is variable. The paper illustrates the power converter design procedure, the hybrid PWM method and the small signal modeling used to design the controllers of each inverter. In addition, the performance of the multilevel converter is verified by means of simulation and experimental results, which show the system ability to operate as expected.**

Keywords—multilevel converters; digital control; renewable sources of energy; distributed generation systems.

I. INTRODUCTION

The utilization of multilevel converters has recently become a frequently adopted solution for high-power and power-quality demanding applications [1]-[3]. The main reasons are the higher voltage operating capability reached with conventional semiconductors, lower common-mode voltages and inherently improved power quality (voltages with reduced harmonic contents and nearly sinusoidal currents).

Among the several application fields of multilevel converter topologies, one of particular interest, nowadays, is the interface of renewable energy sources in distributed generation (DG) systems. An example of this kind of application is the use of the multilevel converters in grid connected PV systems [4]-[8]. In particular, the cascaded H-bridge (CHB) multilevel converter has attracted attention for this application. Indeed, each H-bridge power cell uses isolated DC sources, which can be easily supplied by PV module strings. Furthermore, it offers benefits such as lower switch voltage stress, by interconnecting enough modules in series, and reduced switching frequency, which improves the system efficiency.

Moving along the same line, this paper proposes a grid-connected (127V/60Hz) CHB multilevel converter system that integrates a PV array, considered as the primary energy source, and a battery pack. Because the available energy from PV systems may vary depending on the weather conditions (temperature, solar radiation, partial shading), season, and geographic location, it is indeed interesting to augment the system with an energy storage device, so as to provide a certain degree of power fluctuation compensation, or peak shaving capability [9]. Thereby, the proposed multilevel topology has in its set-up two H-bridge power cells connected in series, one of them, designed to operate at grid frequency, connected to a PV array and the other one, operating in PWM, to a rechargeable battery. Compared with conventional solutions, the one proposed in this paper has two major advantages: *i)* it can use lower voltage switches on each inverter and *ii)* it can exploit line frequency operation in the higher power unit without causing excessive grid current distortion. Besides illustrating the multilevel system topology, this study develops a general methodology and a control strategy to implement the power fluctuation suppression, feeding the grid and the local loads with a constant pre-defined amount of active power at high power factor.

II. MULTLEVEL CONVERTER SYSTEM

The proposed topology is shown in Fig. 1. As can be seen, it uses two H-bridge modules connected in series, being fed by two independent energy sources. Exploiting the inherent flexibility of the topology, where, each of the different H-bridge power cells can process a different power level and operate with a different switching frequency, in the proposed solution the PV powered cell operates at line frequency while the battery connected one, that processes a lower power, is PWM modulated. The converter, therefore, operates as an hybrid PWM modulated system [1], minimizing the switching losses. In addition, thanks to the series connection, the DC-link voltages are minimized as well, allowing the use of reduced voltage switches, again to the benefit of conversion efficiency.

In order to highlight the physical limitations of the cascaded arrangement shown in Fig. 1, we will now analyze it in more detail. In the first place, please note that we assume that the array of PV panels already has a maximum power point tracking control, and the battery pack also has a built-in charging and discharging controller, so that both inverter cells can be assumed to be fed by a voltage source, namely V_{DC_A} and V_{DC_B}. Due to the different physical nature of the sources, inverter A, powered by photovoltaic panels, operates in unidirectional mode, i.e., the whole power generated by the panels will be transferred to the system, whereas inverter B, powered by batteries, operates in a bi-directional mode, so that

This work was sponsored by São Paulo Research Foundation – FAPESP.

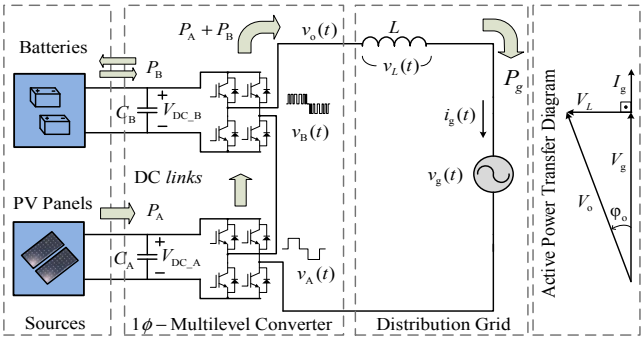

Fig. 1. Single-phase grid-connected multilevel converter interfacing PV pannels and batteries and the active power transfer diagram.

the batteries can be charged or discharged as required. Therefore, the proposed system must manage the power flow so as to make the H-bridge cell A deliver all the active power available from its DC-link, P_A, while the H-bridge cell B operates both as a series active filter, keeping the AC grid current in phase with the grid voltage (with minimal distortion) and as an active power compensator, keeping the power delivered to the grid, and possibly to local loads, as constant as possible, even if variations occur in the input power P_A.

To obtain high power factor at the point of common coupling (PCC), the following condition shall be satisfied: the fundamental component of current flowing through the circuit, defined as I_g, must be in phase with the fundamental component of the distribution system voltage, called V_g. From these considerations, it is possible to establish a diagram, shown in Fig. 1, which represents the desired situation, where I_g and V_g are respectively the phasor representations of the fundamental *rms (root mean square)* grid current and voltage, V_L is the *rms* voltage across the coupling inductor, V_o is the phasor representing the fundamental *rms* output voltage of the multilevel converter, and φ_o is the displacement angle between the grid voltage and the terminal voltage of the cascade multilevel converter. Note that the resultant vector, that represents the output voltage of the multilevel converter, is the sum of the fundamental components of the output voltages generated by the cells A and B, i.e., $V_o=(V_A+V_B)$, where V_A and V_B. represent the *rms* voltage produced by the power cells A and B, respectively. Thus, the vector sum V_A+V_B is expected to produce a resulting vector such that V_L is always at 90° from V_g, to satisfy the condition of maximum transfer of active power, according to (1).

$$V_L = (V_A + V_B) - V_g \tag{1}$$

III. Design Procedure and Control Method

In the previous section, the multilevel topology to be used as an interface of renewable sources and batteries was defined. In this section, analysis and basic procedures to design the multilevel system are presented, which serve to define the optimal values for variables such as DC-link voltages and line coupling inductance.

A. Basic Design Considerations

In order to present the design procedure, only the fundamental components of current and voltages are considered, because, assuming a negligible grid voltage distortion, they almost completely determine the active power flow. Knowing that the nominal grid *rms* voltage is 127 V and its frequency 60 Hz, the following design constraints are imposed: (a) the considered maximum power (P_{Amax}) and minimum power (P_{Amin}) generated by photovoltaic panels are equal to 1.25 kW and 0.75 kW, respectively; (b) the power (P_g) to be transferred to the utility grid is kept equal to 1 kW*. While the physical meaning of P_{Amax} is obvious, the role of P_{Amin} needs to be clarified. P_{Amin} represents the generated power level below which the system cannot deliver the desired power to the grid, without excessively stressing the battery pack.

With a generated power ranging from P_{Amin} to P_{Amax} the active power processed by the inverter B is a function of power P_A, i.e.,

$$P_B(P_A) = P_g - P_A. \tag{2}$$

As aforementioned, the power P_B, processed by inverter B, will be absorbed or supplied by a battery, thus determining charge and discharge phases, according to the variation of the power generated by the photovoltaic panels. However, according to (2), the maximum P_B in magnitude is equal to 250 W, i.e., P_{Bmax} = + 250 W, and P_{Bmin} = – 250 W, so that the system operates as follows:

- When $P_A = P_g$, $P_B = 0$, i.e., when the power generated by the photovoltaic panels is equal to the reference power P_g, the inverter B does not exchange energy;
- When, $(P_g - P_{B\max}) \le P_A < P_g$, $P_B > 0$, i.e., when the power generated by the panels is smaller than the power to be transferred, the inverter B will transfer active power from batteries to the grid (if the batteries state of charge allows that);
- When $P_g < P_A \le P_{A\max}$, $P_B < 0$, i.e., the power transferred to the grid remains constant and the additional power is drained by converter B to charge the batteries (if their state of charge allows that).

Note that for P_A power values outside the range aforementioned, or when the battery state of charge does not allow further power absorption/injection, the reference of power P_g to be transferred to the grid will be changed, so that the system operates properly. In other words, a supervising controller, whose characteristics are not considered in this paper, is required to operate the system in real life conditions.

Considering grid fundamental current and voltage to be in phase, i.e. $\cos(\phi)=1$, V_g = 127 V and a fixed P_g = 1 kW, the *rms* grid current is $I_g = (P_g/V_g) = 7.9\,\text{A}$. The coupling inductor voltage drop is given by $V_L = I_g \cdot j\omega L$, where ω is the angular frequency, L is the inductance and f_g is the grid frequency, 60 Hz.

*The choice of these particular values is actually related to the prototype implementation, described in Section VI. The design procedure, of course, has general validity.

B. Control Strategy for Cell A: Amplitude Modulation

Considering only the fundamental components, a control strategy for the power cell A is outlined. It is based on amplitude modulation at fixed phase. From previous data one can define the absolute minimum value of the fundamental component of the output voltage of inverter A, V_{A1min}

$$V_{A1\,min} = P_{A\,max} / I_g = 158.75\ \text{V}, \tag{3}$$

where $P_{A\ max}$ is the maximum primary source power and I_g is the desired grid current. Please note that (3) assumes the phase shift between V_{A1} and the grid voltage is zero. If a suitably higher value is chosen to prevent saturation, e.g. V_{A1}=160 V, then the phase shift at maximum power will be slightly higher than 0. The exact value can be determined according to the following expression:

$$\varphi_{A\,op} = \cos^{-1}\left(\frac{P_{A\,max}}{I_g \cdot V_{A1}}\right)\cdot\frac{180}{\pi} = 7.167^\circ, \tag{4}$$

where $\varphi_{A\,op}$ is the operation angle of V_A, $P_{A\,max} = 1.25$ kW, $I_g = P_g / V_g$ and $V_{A1} = 160$ V. During operation, the amplitude of the fundamental voltage of the inverter A will vary, while its operating angle will be kept constant at $\varphi_{A\,op}$. The required *rms* values of V_{A1} as a function of input power P_A can be calculated as

$$V_{A1\,op}(P_A) = P_A \Big/ \left(I_g \cdot \cos\left(\varphi_{A\,op}\right)\right), \tag{5}$$

where P_A ranges from 0.75 kW to 1.25 kW. In order to deliver the power coming from the source, cell A will have to modulate its fundamental output voltage according to the following law $V_{A\,op}(P_A) = V_{A1\,op}(P_A)\cdot e^{j\cdot\varphi_{A\,op}}$.

In our implementation, fundamental amplitude modulation is achieved by using a simple line frequency, square wave modulation strategy. Inverter A controller varies the switching angle, α, so as to maintain its DC-link voltage regulated at the given reference. As the output voltage of the inverter A is a three level wave at line frequency (where α represents a half of the zero voltage angular interval), the AC current that flows has large harmonic content. Therefore, it is desirable that the DC-link voltage of inverter A is as small as possible, so that inverter B can more effectively compensate a greater number of harmonics in the current. The design of the DC-link voltage can be made in a simple manner. Using the Fourier relation for determining the fundamental component of a square wave ($\alpha = 0$), one can determine the minimum required DC voltage:

$$V_{DC\_A\_min} = V_{A1}\cdot\sqrt{2}\cdot(\pi/4) \cong 177\ \text{V}. \tag{6}$$

Once again, a slightly higher value is chosen in order to avoid saturations, e.g. V_{DC_A}=180 V. Once V_{DC_A} is determined, one can establish a modulation function that relates the switching angle and power P_A, that is:

$$\alpha(P_A) = \cos^{-1}\left(\frac{V_{A1\,op}(P_A)\cdot\sqrt{2}}{V_{DC\_A}}\cdot\frac{\pi}{4}\right). \tag{7}$$

C. Defining the Parameters for Inverter B

To guarantee current control at all operating points, in the following we establish some relations that directly constrain inductance L and the DC-link voltage V_{DC_B}.

1) According to (1), inverter B needs to supply an *average* voltage given by:

$$V_B(P_A, L) = V_g + V_L(L) - V_{A\,op}(P_A). \tag{8}$$

So, in order to determine V_B, it is necessary to obtain the value of V_L as a function of the inductance L.

2) However, (1) has to be satisfied in every PWM switching period, which means that, during inverter A zero voltage interval, the total $V_o(L)$ will have to be generated by inverter B. Instead, when inverter A is generating a voltage equal to $\pm V_{DC\_A}$, inverter B has to generate, on average, the difference between $V_o(L)$ and V_{DC_A}. Considering both cases, a minimum V_{DC_B} voltage level can be found, assuming $\varphi_{A\,op}$ angle negligible, and is given by:

$$V_{DC\_B}(L) = \max\left\{\begin{matrix}\sqrt{2}V_o(L)\cdot\sin\left(\alpha(P_A)\right)\\ \left|\sqrt{2}V_o(L)\cdot\sin\left(\alpha(P_A)\right) - V_{DC\_A}\right|\end{matrix}\right\}, \tag{9}$$

where $V_o = V_g + V_L$ is the *rms* value of v_o and α is the switching angle of inverter A.

3) The choice of V_{DC_B} and L, finally, affects the design of inverter B also from another standpoint, i.e. harmonic current compensation capability. Indeed, inverter B operates with current control in order not only to adjust grid current fundamental, so as to deliver the maximum active power to the grid, but to compensate distortions as well. Thus, V_{DC_B} voltage must be high enough so that the current control can compensate a reasonable number of harmonics, say up to the 5th or 7th and keep current control without incurring into deep saturation.

The constraints discussed above determine three relationships involving L and V_{DC_B}. Assuming reasonable inductance values, e.g. from 1 mH to 20 mH, in $V_L = I_g \cdot j\omega L$ and substituting in (8) and (9) we could set-up an iterative procedure to determine the minimum operation values of V_B (maximum magnitude values) and V_{DC_B} with respect to L. After the analysis, it was determined that the worst case for constraint 1) is when P_A=P_{Amin} and the worst case for constraint 2) is when P_A=P_{Amax}.

For the constraint 3) we determined the lowest value of V_{DC_B} in order to compensate up to the 7th harmonic component of the current, under the condition which the time derivative of current determined by inverter B is at least equal to the time derivative of current determined by the voltage V_A. Considering the worst cases, V_B and V_{DC_B} are plotted in relation with inductance L in Fig. 2. Observing Fig. 2, we see how $V_{DC\_B} = 170$ V and $L = 10$ mH is a (limit) solution that satisfies all constraints. Lower L values, down to 1 mH, are equally possible, but were not available for the experiments at the time of writing.

Now, extracting the magnitude $|V_B(P_A,L)|$ and the phase angle $\varphi_B(P_A)$ from $V_B(P_A, L)$ for $L = 10$ mH, and given

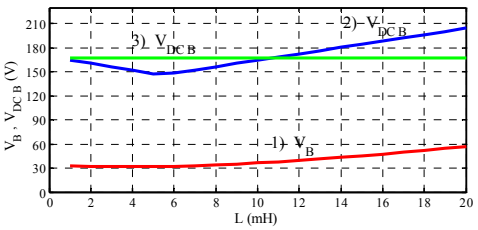

Fig. 2. Magnitudes of V_B and V_{DC_B} with respect to inductance L.

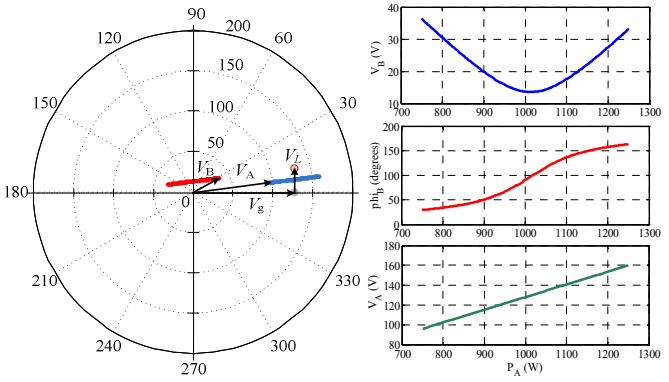

Fig. 3. Amplitude modulation: (a) locus of V_A and V_B to keep current control; (b) magnitude and angle of the voltage the inverter B needs to supply.

$V_{A\,op}(P_A)$, it is possible to obtain the graphics, in Fig. 3, that show the steady-state operation of the multilevel converter with the amplitude modulation strategy applied to inverter A. Fixing the phase angle of phasor V_A and varying its amplitude, as implied by (7), inverter B can exchange energy by varying the angle and amplitude of its fundamental voltage. This can be verified inspecting the *locus* generated by phasors V_A and V_B in Fig. 3(a). Then, it is possible to see that inverter B will have to generate at least the following *rms* voltage (Fig. 3(b)):

$$V_{B\,min} = \left|V_B(P_{A\,min})\right| \cong 37\ \text{V}\,. \tag{10}$$

IV. Design of Control Loops

The multilevel converter operation mode proposed in this paper requires two independent control loops, one to regulate DC voltage of the inverter A, and the other one to control the multilevel output current by inverter B. Both control scheme diagrams and circuit parameters are shown in Fig. 4 and Table I, respectively. In this section, classic design procedures using PI controllers are presented for current and voltage control loops, guaranteeing small steady-state error in tracking the reference current and voltage signals [10].

A. Inverter A: DC Link Voltage Control Loop

Voltage control of the DC-link is performed by adjusting, through switching angle variations, the small amount of real power flowing into the DC-link capacitor. The voltage controller actually determines the amount of power transferred to the system from the DC source, thus compensating for the conduction and switching losses. In steady-state, P_A (power available at the DC-link) has to be equal to the sum of the converter losses and the power transferred to the grid. Please

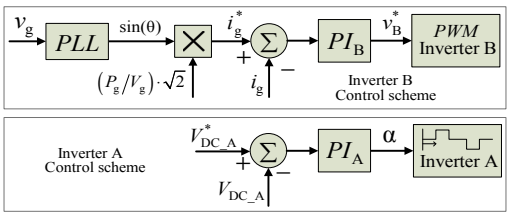

Fig. 4. Control scheme diagrams for inverter A and B.

TABLE I. Multilevel System Parameters

V_{DC_A}	V_{DC_B}	L	V_g	P_g^*	f
180 V 1.42 p.u.	170 V 1.34 p.u.	10 mH 0.234 p.u.	127 V 1.0 p.u.	1000 W 1.0 p.u.	60 Hz
C_A	C_B	P_{Amax}	P_{Amin}	P_{Bmax}	P_{Bmin}
1360 uF 8.27 p.u.	2720 uF 16.54 p.u.	1250 W 1.25 p.u.	750 W 0.75 p.u.	250 W 0.25 p.u.	−250 W −0.25 p.u.

note that we are neglecting the presence of inverter B, as it operates well beyond the control bandwidth considered in this proposal. Disregarding the converter losses, the power balance of the system is as follows:

$$\frac{dE_{C_A}}{dt} = P_A - V_{A1}\cdot I_g\cdot\cos\left(\phi_{A\,op}\right). \tag{11}$$

In (11), $E_{C_A} = (1/2)\cdot C_A\cdot V_{DC\_A}^2$ is the energy stored in the DC-link capacitor C_A. The controlled variable V_{DC_A} is considered to be equal to the superposition of a steady-state component and a perturbation component, $V_{DC\_A} = \overline{V}_{DC\_A} + \tilde{v}_{DC\_A}$. Thus, considering P_A and the grid current I_g constant (steady-state) and solving (11) for small signals yields:

$$C_A\cdot\overline{V}_{DC\_A}\cdot\frac{d}{dt}\tilde{v}_{DC\_A} = -\tilde{v}_{A1}\cdot I_g\cdot\cos\left(\phi_{A\,op}\right) \tag{12}$$

As shown by (7) the relation between the switching angle α, the control variable, and the fundamental voltage of the inverter A is non linear. However, partially deriving $V_{A1}(\alpha)$ in function of V_{DC_A} and α, and rewriting in terms of small signals approximation yields

$$\tilde{v}_{A1} = \frac{4}{\pi\cdot\sqrt{2}}\cdot\cos\left(\bar{\alpha}\right)\cdot\tilde{v}_{DC\_A} - \frac{4\cdot\overline{V}_{DC\_A}}{\pi\cdot\sqrt{2}}\cdot\sin\left(\bar{\alpha}\right)\cdot\tilde{\alpha}\,, \tag{13}$$

where $\bar{\alpha}$ is the steady-state switching angle and $\tilde{\alpha}$ is the small signal controller output. Substituting (13) in (12), simple calculations yield the following result for $G(s) = \left(\tilde{v}_{DC\_A}/\tilde{\alpha}\right)(s)$:

$$G(s) = \overline{V}_{DC\_A}\cdot\tan\left(\bar{\alpha}\right)\cdot\frac{1}{1 + sC_A\cdot\dfrac{\pi\cdot\sqrt{2}\cdot\overline{V}_{DC\_A}}{4\cdot I_g\cdot\cos\left(\bar{\alpha}\right)\cdot\cos\left(\varphi_{A\,op}\right)}}, \tag{14}$$

which is the transfer function between modulation angle $\tilde{\alpha}$ and DC-link voltage. Fig. 5 shows the control loop block diagram. The controller block is represented by a typical proportional integral (PI) regulator structure. Its output represents the switching angle α and G_{TV} is the voltage sensor gain.

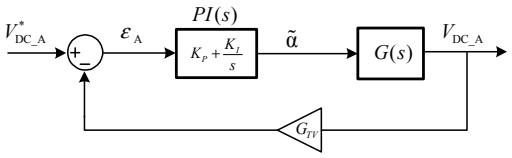

Fig. 5. Control loop block diagram of inverter A.

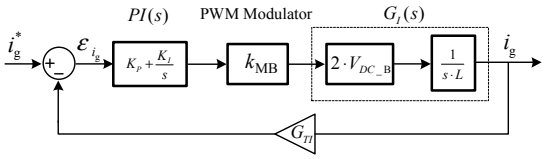

Fig. 6. Current control loop block diagram.

Considering the parameters, C_A=1360 µF, V_{DC_A}=180 V, G_{TV}=1, m_φ=72° (phase margin), $f_{CR\_V}=2$ Hz (crossover frequency), and choosing the peak power case, P_A=P_{Amax}, $\bar{\alpha}=\alpha(P_{A\,max})$, the PI parameters are K_P=3.7e-4 and K_I=0.47 Hz.

B. Inverter B:Current Control Loop

Inverter B operates using a PWM modulation technique to control the grid current i_g. First, the current reference is synchronized with the grid voltage to ensure unity power factor using a PLL [11], [12]. In this case, the reference is constant and is given by:

$$i^*_g(\theta)=\frac{P^*_g}{V_g}\cdot\sqrt{2}\cdot\sin(\theta), \tag{15}$$

where P_g^* is the grid active power reference, V_g is the line voltage, and θ is the synchronous angle produced by the PLL. The error between the generated current i_g and the reference current is processed through a PI controller, and then the output current error is compared with a symmetrical triangular waveform (15 kHz) in order to produce the gate signals.

The transfer function between inverter voltage and grid current is given by:

$$G_I(s)=k_{GI}\cdot\frac{1}{s\cdot L}, \tag{16}$$

where $k_{GI}=2\cdot V_{DC\_B}$ is the gain of the converter and L=10 mH is the coupling inductor. The block diagram of the current control loop for the inverter B is shown in Fig. 6, where all the components are represented for their respective transfer functions or gains. The design of the current control loop gains K_P and K_I was carried out based on the parameters V_{DC_B}=170 V, G_{TI}=1, m_φ=72°, $f_{CR\_I}=(15/6)$ kHz, which yield the following controller constants: K_P=0.44 and K_I=2242 Hz.

V. Simulation Results

The performance of the proposed multilevel converter system has been verified by simulations using PSIM® for the power circuit and control. The control system is implemented as a C script in a discrete time simulation block. A grid-connected cascaded structure has been considered to transfer 1 kW to the grid and also to keep current control. In order to represent the photovoltaic generator, a current source connected to the DC-link of the inverter A was used, and instead of batteries, we used a bi-directional controlled rectifier to deliver or absorb energy and regulate the voltage V_{DC_B}.

Fig. 7 shows the simulation results of the multilevel converter when the input power P_A=750 W. In this case, inverter B is delivering 250 W to the system in order to maintain P_g=1 kW. The current controller behavior can be observed in Fig. 7(a), which shows the grid current in phase with the grid voltage, while Fig 7(b) shows the output voltages of inverters A and B as well as the output of the current controller. Fig. 8 shows the simulation results for an input power P_A=1 kW. Note that the grid current remains controlled while inverter B does not exchange energy with the system. Similarly, Fig 9 shows the results for P_A=1.25 kW. In this case the multilevel converter continues to deliver 1 kW to the grid, and the inverter B is now absorbing 250 W.

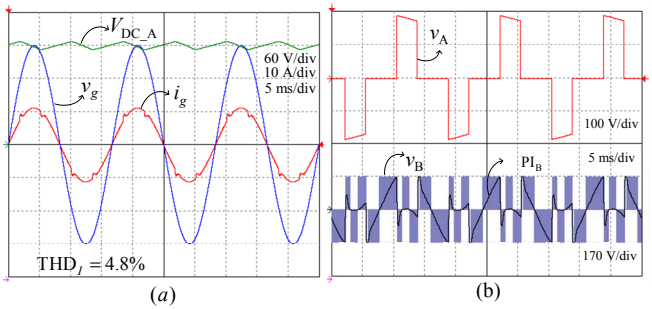

Fig.7. Waveforms for P_A=750 W. (a) grid voltage; grid current; V_{DC_A}. (b) output voltages of inverters A and B; current controller output PI_B.

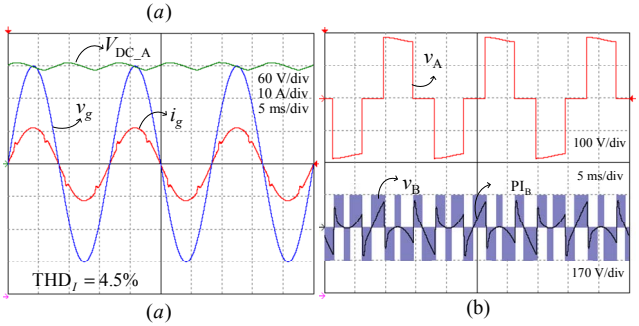

Fig.8. Waveforms for P_A=1 kW. (a) grid voltage; grid current; V_{DC_A}. (b) output voltages of inverters A and B; current controller output PI_B.

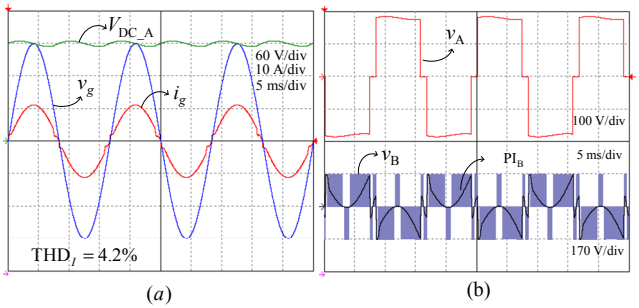

Fig.9. Waveforms for P_A=1.25 kW. (a) grid voltage; grid current; V_{DC_A}. (b) output voltages of inverters A and B; current controller output PI_B.

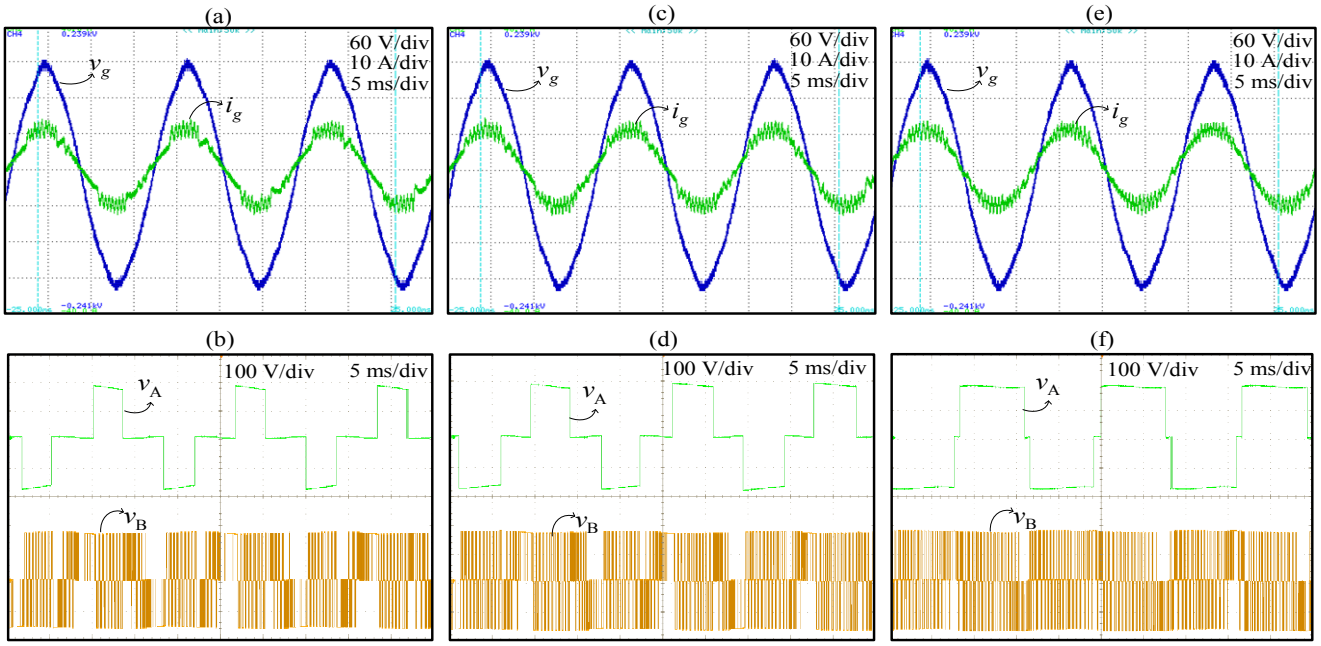

Fig.10. Waveforms for P_A≈750 W: (a), (b); P_A≈1 kW: (c), (d); P_A≈1.25 kW: (e), (f); grid voltage and current (v_g, i_g) ; voltages of inverters A and B (v_A, v_B) .

VI. Experimental Results

After simulation, a hardware prototype of the proposed converter was set-up and experimentally tested in connection to a 127 V/60 Hz power grid. Each H-bridge cell is implemented using modules from SEMIKRON®. The multilevel converter prototype switches at 15 kHz and is controlled by a digital signal processor (TMS320F28335). For practical reasons, the converter is fed by a 4 kW PV source emulator from Magna Power® to represent the PV system and by a bi-directional controlled rectifier to represent the batteries.

Fig. 10 shows the experimental results of the system delivering constant power to the grid. The results were obtained under the same conditions of the simulations, i.e., the DC power of inverter A was adjusted to deliver approximately 750 W, 1.0 kW and 1.25 kW. As can be seen, the multilevel system is able to maintain the current in phase with the grid voltage, to satisfactorily compensate the harmonic distortion and, finally, to control the DC-link voltage of inverter A by adjusting the switching angle.

VII. Conclusion

This paper has described a control method for a multilevel converter connected to grid that can be powered by PV panels and batteries. Independent controllers for each H-bridge power cell were designed and through the simulation and experimental results it was found that even with variations in the power of inverter A DC-link, the multilevel converter was able to transfer a preset power and maintain its output current in phase with the grid voltage.

References

[1] J. Rodriguez, S. Bernet, W. Bin, J. O. Pontt, and S. Kouro, "Multilevel Voltage-Source-Converter Topologies for Industrial Medium-Voltage Drives," *IEEE Trans. Ind. Electron.*, vol. 54, pp. 2930-2945, 2007.

[2] L. G. Franquelo, J. Rodriguez, J. I. Leon, S. Kouro, R. Portillo, and M. A. M. Prats, "The age of multilevel converters arrives," *IEEE Industrial Electronics Magazine*, vol. 2, pp. 28-39, 2008.

[3] J. Rodriguez, L. G. Franquelo, S. Kouro, J. I. Leon, R. C. Portillo, M. A. M. Prats, and M. A. Perez, "Multilevel Converters: An Enabling Technology for High-Power Applications," *Proceedings of the IEEE*, vol. 97, pp. 1786-1817, 2009.

[4] S. Daher, J. Schmid, and F. L. M. Antunes, "Multilevel Inverter Topologies for Stand-Alone PV Systems," *IEEE Transactions on Industrial Electronics*, vol. 55, pp. 2703-2712, 2008.

[5] S. A. Khajehoddin, A. Bakhshai, and P. Jain, "The Application of the Cascaded Multilevel Converters in Grid Connected Photovoltaic Systems," at IEEE Electric Power Conference. EPC 2007. Canada 2007.

[6] E. Ozdemir, S. Ozdemir, and L. M. Tolbert, "Fundamental-Frequency-Modulated Six-Level Diode-Clamped Multilevel Inverter for Three-Phase Stand-Alone Photovoltaic System," *IEEE Transactions on Industrial Electronics*, vol. 56, pp. 4407-4415, 2009.

[7] J. Selvaraj and N. A. Rahim, "Multilevel Inverter For Grid-Connected PV System Employing Digital PI Controller," *IEEE Transactions on Industrial Electronics*, vol. 56, pp. 149-158, 2009.

[8] E. Villanueva, P. Correa, and J. Rodriguez, "Control of a single phase H-Bridge multilevel inverter for grid-connected PV applications," presented at 13th Power Electronics and Motion Control Conference. EPE-PEMC 2008., 2008.

[9] H. Fakham, P. Degobert, and B. Francois, "Control system and power management for a PV based generation unit including batteries," presented at International Aegean Conference on Electrical Machines and Power Electronics, 2007. ACEMP '07, 2007.

[10] M. H. Rashid, *Power Electronics Handbook*: Academic Press, 2001.

[11] F. P. Marafão, S. M. Deckmann, J. A. Pomilio, and R. Q. Machado, "Metodologia de projeto e análise de algoritmos de sincronismo pll," *SOBRAEP Revista da Associação Brasileira de Eletrônica de Potência*, vol. 10, pp. 7-14, 2005.

[12] J. Rocabert, G. M. S. Azevedo, A. Luna, J. M. Guerrero, J. I. Candela, and P. Rodríguez, "Intelligent Connection Agent for Three-Phase Grid-Connected Microgrids," *IEEE Transactions on Power Electronics*, vol. 26, pp. 2993-3005, 2011.